ACS OMEGA

http://pubs.acs.org/journal/acsodf

Article

Amphiphilic mPEG-Modified Oligo-Phenylalanine Nanoparticles Chemoenzymatically Synthesized via Papain

Feng Wang,* Youhua Li, Lu Yu, Jinwen Zhu, Fuming Zhang, and Robert J. Linhardt

Cite This: *ACS Omega* 2020, 5, 30336−30347

Read Online

ACCESS | Metrics & More | Article Recommendations | Supporting Information

ABSTRACT: Amphiphilic mPEG-modified peptide nanoparticles were developed from oligo-phenylalanine (OPhe) nanoparticles (NPs) synthesized via papain. Tyndall effects indicate that OPhe NPs are amphiphobic. Addition of protein perturbants, sodium dodecyl sulfate (SDS), and urea, in the dispersion solution of OPhe NPs can significantly reduce the $R_{h,m}$ value of NPs, from approximately 749.2 nm to about 200 nm. Therefore, the hydrophobic interaction and hydrogen bonding play major roles in maintaining the aggregation of OPhe NPs. Using the "grafting to" method, the methoxypolyethylene-modified OPhe NPs (mPEG-*g*-OPhe NPs) were synthesized and characterized by Fourier transform infrared spectroscopy (FTIR), ^{1}H NMR, electrospray ionization mass spectrometry (ESI-MS), and dynamic light scattering (DLS). The attenuated total reflectance (ATR) spectrum of OPhe NPs and mPEG-*g*-OPhe NPs demonstrate that the secondary structures of these NPs are mainly β-type. mPEG-*g*-OPhe NPs can self-aggregate into spherical micelles both in water and cyclohexane. Increasing the chain length of the mPEG moiety, the critical micellar concentrations of mPEG-*g*-OPhe NPs increased in water but decreased in cyclohexane. The light stability, thermal stability, hydrolysis stability, and encapsulation stability of curcumin were significantly promoted by encapsulation in the micelles formed by mPEG-*g*-OPhe NPs. The protective effects regularly varied with the variations in the mPEG chain length of mPEG-*g*-OPhe NPs.

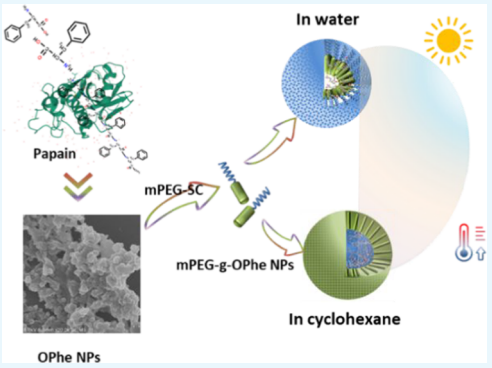

INTRODUCTION

Peptides constitute a rapidly growing class of materials in different fields from electronic to nanomedicine.[1,2] Solid or liquid phase peptide synthesis methods are well established for the preparation of peptides from specific amino acids.[3,4] Due to the required protection/deprotection and coupling steps and the use of toxic solvents, chemical syntheses generally result in high-cost processes. Recombinant protein expression allows protein engineering of desired sequences into microorganisms and production by fermentation. However, microorganisms often poorly express repetitive peptides, especially cationic or hydrophobic peptides.[5] Enzymatic polymerization catalyzed by proteases has the advantage of conducting the polymerization in an aqueous medium (i.e., in buffer solutions) under mild conditions, representing greener polymerization processes.[6,7] The polymerization of amino acid monomers via proteases can be carried out under thermodynamic control or kinetic control.[8] In kinetically controlled polymerization reactions, hydrophobic amino acid monomers are suitable substrates due to the high affinity shown by proteases for hydrophobic amino acids.[6] The hydrophobic nature of amino acids, including L-phenylalanine, makes the resulting polypeptides insoluble in water, leading to precipitation during the polymerization process and shifting the equilibrium toward peptide formation.[6]

Peptides are inherently biocompatible and biodegradable to natural metabolites since amino acids are intrinsic components of the human body. PEGylation can improve the water solubility and stability of peptides in vivo administration and reduction of immunogenity.[9] PEGylated peptides are able to self-assemble to form various superstructures like nanotubes, micelles, fibrils, and organogels.[10−14] In recent years, peptide nanoparticles (NPs) derived from amino acid-based precursors have been attracting interest in the fields of biomedicine and nanobiotechnology.[15−17] Peptide building blocks, such as cyclic peptides,[18] aromatic dipeptides,[19] surfactant-like oligopeptides,[20] and cationic dipeptides,[21] display a promising potential in the development of peptide nanoparticles. Various methods of hydrolysis, crosslinking, and solvent exchange have been used for the preparation of peptide nanoparticles. For instance, Zhang et al. fabricated soy peptide nanoparticles from large peptide aggregates during hydrolysis of soy protein isolates.[16] Lipid oxidation in emulsions stabilized by the soy peptide nanoparticles was suppressed. Yaman et al. and Zhang et al. synthesized diphenylalanine-based NPs using the crosslinking method with aldehydes.[22,23] The NPs have

Received: October 17, 2020
Accepted: October 28, 2020
Published: November 10, 2020

Scheme 1. Preparation of mPEG-*g*-OPhe NPs and the Micellar Self-Aggregation of the NPs[a]

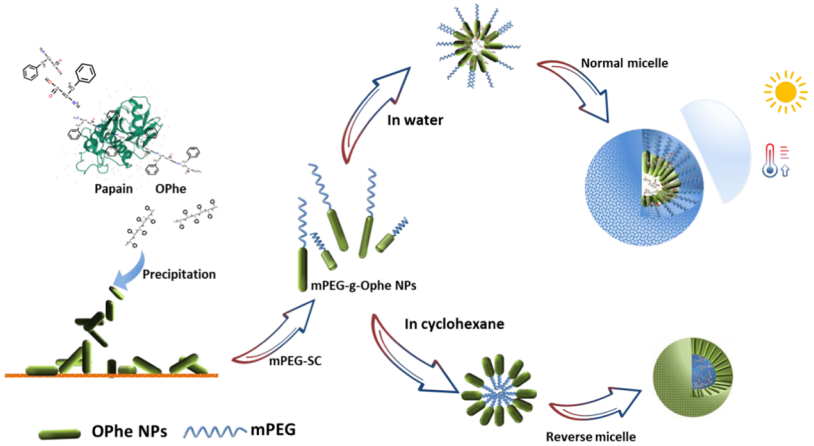

[a]OPhe NPs, oligo-phenylalanine nanoparticles; mPEG-*g*-OPhe NPs, methoxypolyethylene glycol-modified oligo-phenylalanine NPs; and mPEG-SC, methoxypolyethylene glycol succinimidyl carbonate ester.

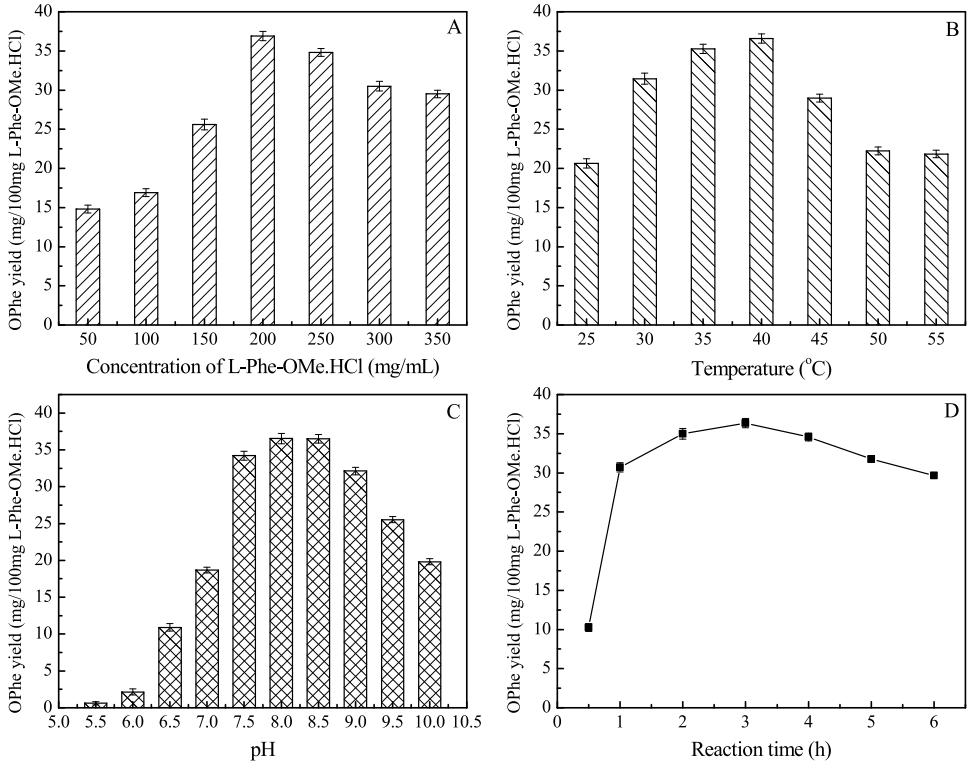

Figure 1. Influences of various L-Phe-OMe·HCl concentrations (A), temperatures (B), pHs (C), and reaction times (D) on the amount of OPhe NPs produced per 100 mg of L-Phe-OMe·HCl at 4 U/mL papain and 15% (v/v) DMSO in the buffer (200 mmol/L).

potential applications in electrochemical cytosensors and cancer treatment. In the study of Dittrich et al., it was found that the hydrophobic 10 amino acid peptides assembled into solid particles when the solvent was exchanged from ethanol to water.[24]

Tethering soluble tails on polymeric nanoparticles produces amphiphilic tailed polymeric nanoparticles, which have been attracting intense focus owing to their easily tunable dimensions and properties.[25,26] Herein, oligo-phenylalanine nanoparticles (OPhe NPs) synthesized via papain were modified with soluble methoxypolyethylene (mPEG) to produce the amphiphilic nanoparticles of mPEG-*g*-OPhe. The mPEG-*g*-OPhe NPs can self-aggregate into micelles in water and an organic medium (Scheme 1). To our knowledge, the characterization of peptide nanoparticles synthesized by enzymatic polymerization has not yet been reported.

RESULTS AND DISCUSSION

Synthesis and Characterization of OPhe NPs and mPEG-*g*-OPhe NPs. Polymerization of L-phenylalanine methyl ester hydrochloride (L-Phe-OMe·HCl) via papain utilizes the native functions of the protease to promote the reverse hydrolysis reaction, aminolysis. Papain is commercially available, inexpensive, and extracellularly stable, showing a high affinity for hydrophobic amino acids like L-Phe. The synthesis of polypeptides catalyzed by papain is under kinetic control.[6,27]

https://dx.doi.org/10.1021/acsomega.0c05076
ACS Omega 2020, 5, 30336−30347

The yield of the kinetically controlled reaction is in direct relationship with the enzyme/substrate ratio.[28,29] The effect of various concentrations of the monomer (L-Phe-OMe·HCl) on the amount of OPhe NPs produced per 100 mg of L-Phe-OMe·HCl was investigated under the conditions of 4 U/mL papain, 15% (v/v) dimethyl sulfoxide (DMSO) in the buffer (pH 8.0, 200 mmol/L) at 40 °C for 3 h. The results are shown in Figure 1A. The yield reached the maximal value (36.9 ± 0.6 mg/100 mg L-Phe-OMe·HCl) at 200 mg/mL L-Phe-OMe·HCl. When the monomer concentration was increased to be higher than 200 mg/mL, the reduction in the yield of OPhe NPs was observed, indicating that substrate inhibition occurred.[30] Similar results were reported by Yang and co-workers in their study of α-chymotrypsin-catalyzed oligomerization of oligo(Et-Asp) synthesis.[31]

Temperature is one important factor impacting the balance between hydrolysis and condensation (reverse hydrolysis) catalyzed by protease.[32] The effect of temperature on the synthesis of OPhe NPs via papain was examined in the temperature range from 25 to 55 °C at 4 U/mL papain, 15% (v/v) DMSO in the buffer (pH 8.0, 200 mmol/L), at 40 °C for 3 h (Figure 1B). The product yield increased with the increase of temperature below 40 °C. When the temperature rose higher than 40 °C, the product yield reduced. This may be due to the increased hydrolysis rate of ester and peptide at higher temperatures. According to the scheme of kinetically driven protease-catalyzed peptide synthesis,[33] the OPhe polymer was synthesized through the formation and deacylation of an enzyme−acyl intermediate, involving the carbonyl of activated amino acid at the protease active site. Thus, the pH effect is crucial in this nucleophilic process of oligo-peptide formation. Figure 1C demonstrates the impact of various initial pHs on the OPhe NP synthesis. The maximum yield was obtained at pH 8.0 when polymerization was catalyzed by 4 U/mL papain in the buffer (200 mmol/L) of 15% (v/v) DMSO at 200 mg/mL L-Phe-OMe·HCl and 40 °C for 3 h. The time course of the OPhe synthesis was plotted (Figure 1D) under reaction conditions of 4 U/mL papain, 200 mg/mL L-Phe-OMe·HCl, and 15% (v/v) DMSO in phosphate buffer (pH 8.0, 200 mmol/L) at 40 °C. The yield of OPhe NPs reached the maximum value in 3 h. Then, a decrease in the yield occurred during extended reaction times. This may be due to the protease-catalyzed hydrolysis of ester or amide groups of OPhe NPs converting them to the water-soluble coproduct.[31]

The polymerization of amino acid monomers catalyzed by a protease is often deliberately conducted in a nonaqueous reaction medium containing cosolvents such as dimethyl sulfoxide, acetonitrile (ACN), etc.[34] The presence of co−solvents reduces the dielectric constant and hydration degree of the reaction medium inhibiting the side reactions.[35] Furthermore, the solubility of the amino acid polymer will be increased by the addition of cosolvents promoting the polymerization.[36] The effect of the addition of different cosolvents on the OPhe NP synthesis catalyzed by papain is shown in Figure 2. The polymerization was promoted by addition of DMSO in the concentration range of 5−25% (v/v). Compared with that obtained in the case without cosolvent addition, the yield of OPhe NPs was increased maximally by about 130% when the reaction was conducted using 4 U/mL papain, 200 mg/mL L-Phe-OMe·HCl, and 15% (v/v) DMSO in the buffer (pH 8.0, 200 mmol/L), at 40 °C for 3 h. The additions of DMF, ACN, Diox, MeOH, hexafluoroisopropanol (HFIP), and tetrahydrofuran (THF) in the concentration

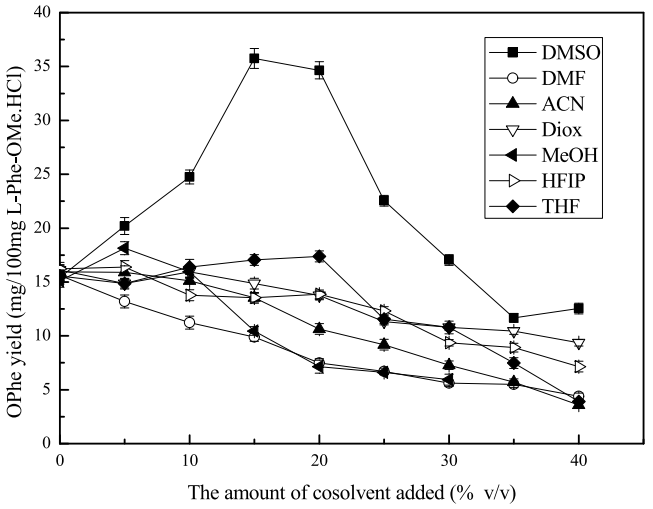

Figure 2. Addition of cosolvents on the OPhe NP yield via papain. Reaction conditions: 200 mg/mL L-Phe-OMe·HCl, 4 U/mL papain, in 3.0 mL of phosphate buffer (pH 8.0, 200 mmol/L), at 40 °C, for 3 h.

range of 5−40% (v/v) showed negative effects on the OPhe NP yield.

The polymerization degree (DP) of OPhe NPs dissolved in deuterated dimethyl sulfoxide (DMSO-d_6) was estimated using ^{1}H NMR (Figures S1−S11). The average polymerization degree (DP_{avg}) of OPhe was determined by comparing the ratio of protons of $ArCH_2$- (2.6−3.1 ppm) to the $-OCH_3$ (3.56−3.57 ppm). According to the results listed in Table S1, the DP_{avg} value fluctuated in a relatively narrow range of 4.26−5.79 when the pH, temperature, and the type of cosolvent varied. Electrospray ionization mass spectrometry (ESI-MS) analysis was performed for OPhe NPs obtained under the conditions when the yield of OPhe NPs reached the maximal value. The reaction was carried out using 4 U/mL papain, 200 mg/mL L-Phe-OMe·HCl, and 15% (v/v) DMSO buffer (pH 8.0, 200 mmol/L) at 40 °C for 3 h. The ESI-MS analysis demonstrates that the ion peaks in the spectrum are separated by 147 m/z unit, which is equal to the mass of Phe repeat units (Figure S15A). The main molecular ions observed for OPhe are m/z 768.3 and 915.2 corresponding to the pentapeptide and hexapeptide, respectively.

The hydrophobic nature of L-Phe induces the precipitation of OPhe NPs during the polymerization process. As the scanning electron microscopy (SEM) images and transmission electron microscopy (TEM) photo display in Figure 3, the OPhe NPs formed during the polymerization are irregularly shaped nanoparticles (NPs). Dynamic light scattering (DLS) measurement demonstrates that the hydrodynamic mean diameter ($R_{h,m}$) of OPhe NPs is approximately 749.2 nm (Figure 3C). The relatively smaller particle size revealed by SEM and TEM images is due to the air-drying process during sample preparation.[16]

After 2 h of ultrasonic treatment, the Tyndall phenomenon of the OPhe NP dispersion in water is clearly visible by illuminating with a laser pointer (the inset of Figure 3A). The Tyndall effect takes place in a colloidal solution that contains particles with sizes less than the wavelength of the visible light.[37] The Tyndall effect of the OPhe NP dispersion in organic media, such as cyclohexane (CyH), Diox, chloroform ($CHCl_3$), MeOH, and DMSO were also investigated and the

https://dx.doi.org/10.1021/acsomega.0c05076
ACS Omega 2020, 5, 30336−30347

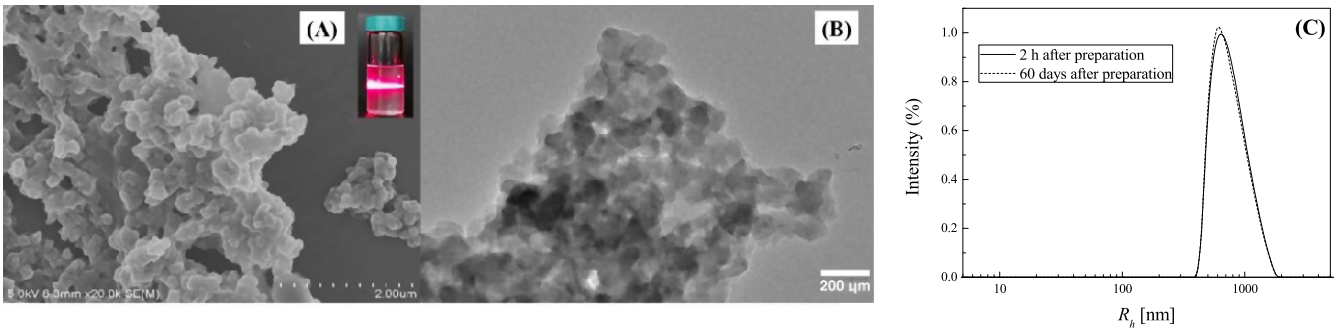

Figure 3. SEM images and the Tyndall phenomenon (A), TEM photo (B), and size distributions (C) of the OPhe NP dispersion in water (0.04 mg/mL) at 25 °C and pH 7.0.

results are shown in Figure 4. Typical Tyndall phenomena are clearly detected for OPhe NP dispersions in CyH, Diox,

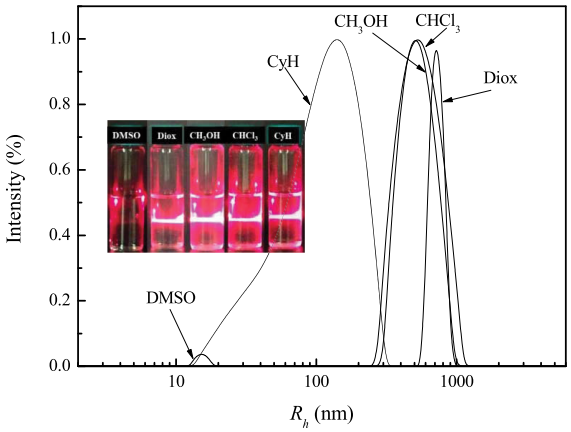

Figure 4. Size distributions and Tyndall phenomena of the OPhe NP (0.04 mg/mL) dispersion in dimethyl sulfoxide (DMSO), dioxane (Diox), methanol (MeOH), chloroform ($CHCl_3$), and cyclohexane (CyH) at 25 °C.

$CHCl_3$, and MeOH. The disappearance of the Tyndall effect in the case of DMSO indicates the dissolution of OPhe NPs in DMSO. This result is consistent with the report that the Phe polymer is one of the most hydrophobic polymers among polymers composed only of amino acids.[38]

Sodium dodecyl sulfate (SDS) and urea are protein perturbants, which can disrupt hydrophobic interaction and hydrogen bonding between peptide chains.[39,40] According to the results shown in Figure 5, the OPhe NP (0.4 mg/mL) dispersion in water turns transparent after the addition of SDS and urea, alone or in combination, indicating the disruption of aggregation of OPhe NPs. The presence of SDS and urea led to a significant reduction ($p < 0.05$) in the value of $R_{h,m}$ of OPhe NPs. Therefore, the hydrophobic interaction and hydrogen bonding plays the major role in maintaining the aggregation of OPhe NPs in water. It is reasonable to infer that the size of OPhe NPs can be as small as 200−250 nm.

After the preparation of OPhe NPs using papain, mPEG-SC was used to modify the N-terminal of OPhe in a methanol suspension of OPhe NPs. The mPEG-*g*-OPhe NPs synthesized in this way possess two chemically distinct regions: the soluble mPEG region and amphiphobic OPhe NP region (Scheme 1). Each gram of OPhe NPs was converted to approximately 1.03 ± 0.05 g of $mPEG_{200}$-*g*-OPhe NPs, 1.15 ± 0.12 g of $mPEG_{400}$-*g*-OPhe NPs, and 1.65 ± 0.15 g of $mPEG_{1000}$-*g*-OPhe NPs. The

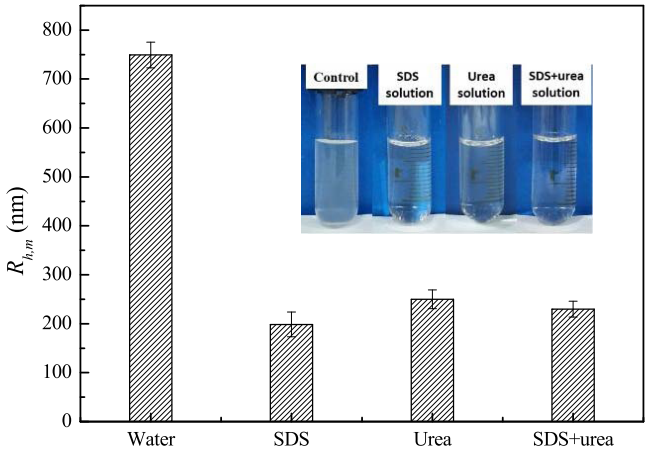

Figure 5. Influence of the addition of protein perturbants of SDS (4% w/v) and urea (8 mol/L) on the $R_{h,m}$ value and visual appearance of the OPhe NP dispersion in water (0.4 mg/mL) at 25 °C and pH 7.0.

dispersion solution of the mPEG-*g*-OPhe NPs show clear Tyndall phenomena upon laser irradiation (the inset of Figure 6A,B). There was an obvious reduction in the value of $R_{h,m}$ of OPhe NPs in water after the mPEG modification. The $R_{h,m}$ values of $mPEG_{200}$-*g*-OPhe NPs, $mPEG_{400}$-*g*-OPhe NPs, and $mPEG_{1000}$-*g*-OPhe NPs in water are determined to be 150.5 ± 10.6, 210.6 ± 22.4, and 255.3 ± 19.5 nm, respectively (Figure 6A). The increased hydrophilicity of OPhe NPs after the mPEG modification may weaken the $\pi-\pi$ stacking and hydrophobic interaction between peptide chains, disrupting the aggregation of OPhe NPs. The mPEG-modification of OPhe NPs had no obvious effects on the $R_{h,m}$ value of the NPs dispersed in cyclohexane (Figure 6B). This may be due to the shrinkage and fusion of hydrophilic mPEG chains in cyclohexane.

Fourier transform infrared (FTIR) spectra before and after the introduction of mPEG into OPhe NPs (Figure S16) demonstrate that the peak at 1550 cm^{-1} (N−H inplane deformation) vanishes after the introduction of mPEG, indicating the successful modification of the N-terminal amino group of OPhe NPs. The intensity of the peak at about 1110 cm^{-1} (C−O stretch from the ether group) increases with the increase of the average molecular weight (MW) of mPEG introduced to OPhe NPs. The amide I region of attenuated total reflectance (ATR) FTIR spectra of the NPs was analyzed by peak resolution to further define the structure of OPhe NPs and mPEG-*g*-OPhe NPs. The spectra of OPhe NPs, $mPEG_{200}$-*g*-OPhe NPs, and $mPEG_{400}$-*g*-OPhe NPs reveal

https://dx.doi.org/10.1021/acsomega.0c05076
ACS Omega 2020, 5, 30336−30347

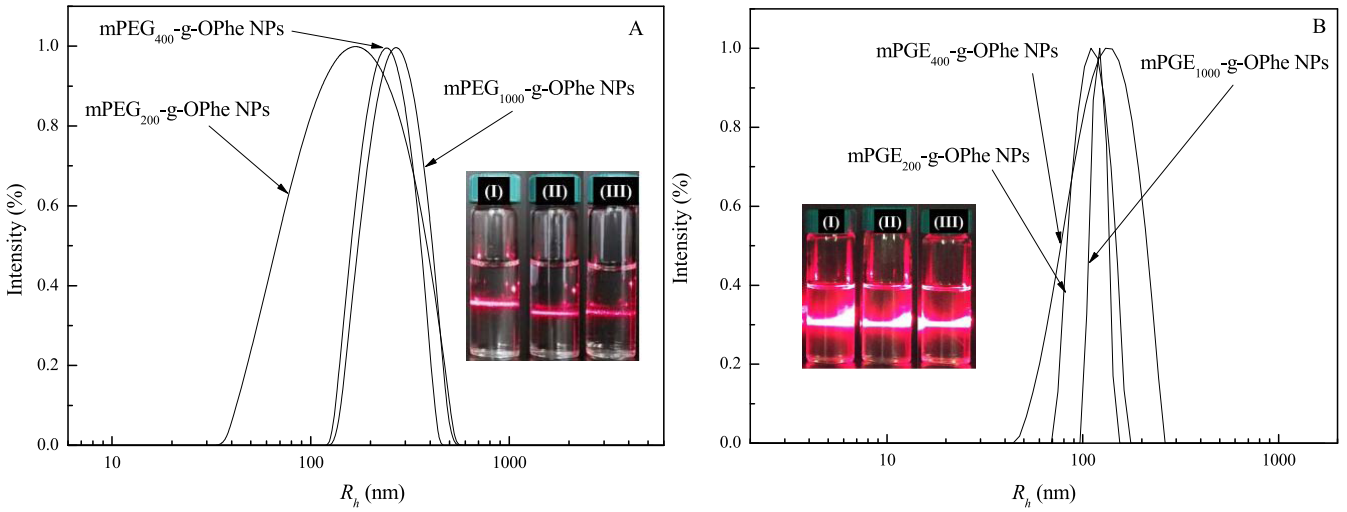

Figure 6. Size distributions and Tyndall phenomena of $mPEG_{200}$-*g*-OPhe NP (I), $mPEG_{400}$-*g*-OPhe NP (II), and $mPEG_{1000}$-*g*-OPhe NP (III) dispersions in water (0.04 mg/mL) (A) and cyclohexane (0.04 mg/mL) (B) at 25 °C and pH 7.0.

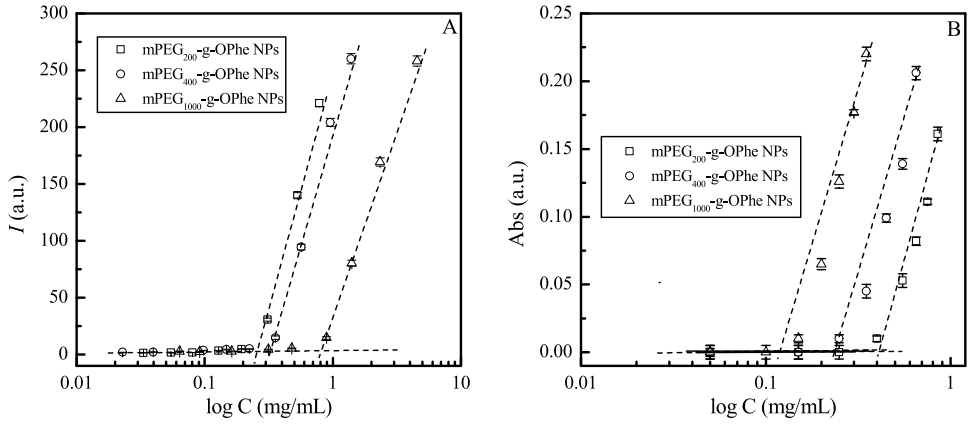

Figure 7. Fluorescence intensity at λ_{max} = 642 nm for excitation spectra of Nile Red as a function of the concentration of the mPEG-*g*-OPhe NP dispersion in water at 25 °C and pH 7.0 (A) and plots of absorbance of iodine as a function of the concentration of the mPEG-*g*-OPhe NP dispersion in cyclohexane (B) at around 370 nm and 25 °C for determining the critical concentration of the normal micelle (A) and reverse micelle (B) at 25 °C. Each value represents the mean ± standard deviation (SD), n = 3.0.

that the secondary structures of these NPs contain β-turns and β-strands (Figures S17−S19).[41] The contents of β-turns and β-strands are 32.8 and 67.2% for OPhe NPs, 29.3 and 70.7% for $mPEG_{200}$-*g*-OPhe NPs, and 32.8 and 67.2% for $mPEG_{400}$-*g*-OPhe NPs (Table S2), respectively. When MW of the mPEG moiety of mPEG-*g*-OPhe NPs was increased to be 1000, the secondary structure of $mPEG_{1000}$-*g*-OPhe NPs consists of 36.3% β-turns, 35% aggregated strands, 16.4% antiparallel β-sheets, and 12.3% β-type structures (Figure S20 and Table S2). The benefit of formation of β-sheet elements is the formation of homogeneous and stable structures.[42] With the increase of the mPEG chain length, the hydrogen bonding site (−O−) contained in the repeat unit significantly increases, contributing to the intermolecular hydrogen-bonded β-sheet associated with aggregation (aggregated strands).[43,44]

According to ESI-MS spectra, the substantial differences in chain-length distributions of $mPEG_{200}$-*g*-OPhe (Figure S15B), $mPEG_{400}$-*g*-OPhe (Figure S15C), and $mPEG_{1000}$-*g*-OPhe (Figure S15D) are owing to the wide MW distribution of OPhe and mPEG. The degree of substitution (DS) of $mPEG_{200}$, $mPEG_{400}$, and $mPEG_{1000}$ on the N-terminal of Ophe NPs was determined by ^{1}H NMR (Figures S12−S14). The DS value of $mPEG_{200}$, $mPEG_{400}$, and $mPEG_{1000}$ was estimated to be about 1 by comparing the ratio of the methoxyl proton of mPEG (3.23−3.25 ppm) to the methoxyl proton of OPhe (3.73−3.74 ppm). Thus, MWs of $mPEG_{200}$-*g*-OPhe, $mPEG_{400}$-*g*-OPhe, and $mPEG_{1000}$-*g*-OPhe were estimated to be 881.2, 1090.4, and 1618.6 g/mol, respectively.

Normal and Reverse Micelles Formed by mPEG-*g*-OPhe NPs. The self-aggregation of mPEG-*g*-OPhe NPs in water was studied with Nile red as the fluorescent probe. The dependence of the Nile red fluorescence intensity at its maximum emission wavelength (λ_{max} = 642 nm) on the concentration of mPEG-*g*-OPhe NPs is plotted in Figure 7A. From the plots, the fluorescence intensity of Nile red is quite weak below certain concentrations indicating that Nile red is in water and few micelles are present. After that, the markedly increased intensities reveal the formation of micelles and the preferential partitioning of Nile red molecules into the core of the micelles. The concentration at the inflection point corresponds to the critical micellar concentration (CMC). Nile red molecules preferentially partition into the hydrophobic core of the micelles driven by the force of hydrophobic interactions due to the $\pi-\pi$ interaction between benzene

https://dx.doi.org/10.1021/acsomega.0c05076
ACS Omega 2020, 5, 30336−30347

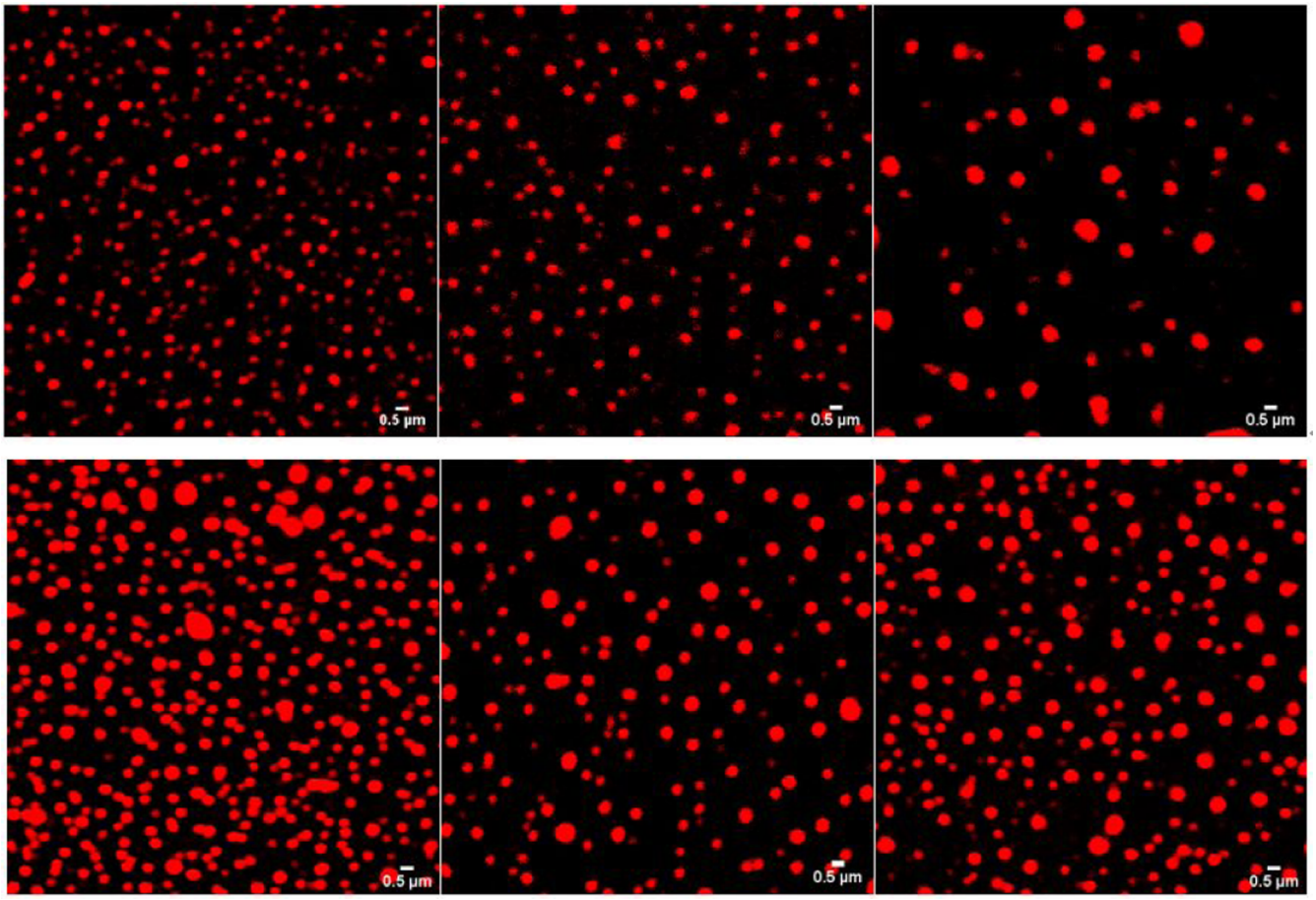

Figure 8. CLSM images of Nile red-loaded mPEG-*g*-OPhe NP micelles in water at λ_{exc} = 543 nm (upper row) at 25 °C and pH 7.0 and Rhodamine B-loaded mPEG-*g*-OPhe NP micelles in cyclohexane at λ_{exc} = 552 nm (bottom row) at 25 °C. The concentration of $mPEG_{200}$-*g*-OPhe NP, $mPEG_{400}$-*g*-OPhe NP, and $mPEG_{1000}$-*g*-OPhe NP dispersions in water (upper row) from left to right: 0.3, 0.5, and 1.0 mg/mL, respectively. The concentration of $mPEG_{200}$-*g*-OPhe NP, $mPEG_{400}$-*g*-OPhe NP, and $mPEG_{1000}$-*g*-OPhe NP dispersions in cyclohexane (bottom row) from left to right: 0.45, 0.25, and 0.15 mg/mL, respectively.

rings.[45,46] According to the results shown in Figure 7A, the CMC of $mPEG_{200}$-*g*-OPhe NPs, $mPEG_{400}$-*g*-OPhe NPs, and $mPEG_{1000}$-*g*-OPhe NPs are 0.25 ± 0.02, 0.33 ± 0.02, and 0.85 ± 0.03 mg/mL, respectively.

Considering that OPhe NPs are amphiphobic solid particles, we speculated about the possibility of the self-assembly of amphiphilic mPEG-*g*-OPhe NPs into reverse micelles in CyH driven by the interfacial free energy between the hydrophilic mPEG chain and CyH. The formation of reverse micelles of mPEG-*g*-OPhe NPs in CyH was examined by the iodine solubilization method.[47,48] With the increase of the mPEG-*g*-OPhe NP concentration in the CyH containing iodine (0.006 mg/mL), a new absorption peak appeared at about 370 nm (Figures S21−S23). The formation of iodine-encapsulated micelles stabilized by mPEG-*g*-OPhe NPs gave rise to the new peak owing to an n-σ electron donor−acceptor interaction.[47] Figure 7B displays the plot of the absorbance of iodine at 370 nm against the concentration of mPEG-*g*-OPhe NPs in CyH at 25 °C. The points of discontinuous changes in the plots are defined as the critical reverse micelle concentrations (CRMCs). The absorbance increased remarkably above CRMC indicating the formation of reverse micelles. According to the results shown in Figure 7B, the CRMCs for $mPEG_{200}$-*g*-OPhe NPs, $mPEG_{400}$-*g*-OPhe NPs, and $mPEG_{1000}$-*g*-OPhe NPs are 0.42 ± 0.01, 0.24 ± 0.02, and 0.12 ± 0.01 mg/mL, respectively. With the increase of the mPEG chain length, more hydrophilic segments of mPEG-*g*-OPhe NPs are exposed to the surrounding solvent, elevating the unfavorable entropy contribution and promoting the formation of reverse micelles at a lower CRMC.

The formation of spherical mPEG-*g*-OPhe NPs micelles in water (Figure 8 upper row) and cyclohexane (Figure 8 bottom row) were verified by confocal laser scanning microscopy (CLSM). The efforts to characterize OPhe NPs dispersed in solution using CLSM failed. The combination of a low quantum yield and low molar extinction coefficient makes phenylalanine to be hardly detectable.[49] The unstable aggregation of OPhe NPs in solution, which cannot accommodate a fluorophore, may also account for the failed confocal imaging. The sizes of micelles formed by mPEG-*g*-OPhe NPs were obtained using Nano Measurer software.[50] According to the results (Table S3), the average diameter of normal micelles increased by about 72.6% when the MW of the mPEG moiety of the NPs increased from 200 to 1000. In water, the hydrophilic chain of mPEG is extended. Therefore, the size of micelles increased with the increase of the chain length of the mPEG moiety of the NPs. On the other hand, the steric effect between mPEG chains increases with the increase of the chain length demanding more OPhe to stabilize the hydrophobic core of the micelles.[51,52] Thus, CMC for the

https://dx.doi.org/10.1021/acsomega.0c05076
ACS Omega 2020, 5, 30336−30347

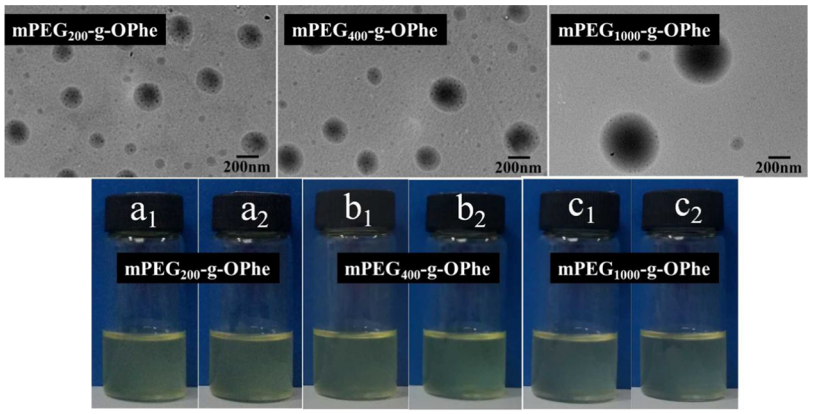

Figure 9. TEM images and appearances of Cur-loaded micelles stabilized by mPEG-*g*-OPhe NPs taken at 1 h (a1, b1, and c1) and 30 days (a2, b2, and c2) after preparation at 25 °C and pH 7.0, respectively. The concentrations of $mPEG_{200}$-*g*-OPhe, $mPEG_{400}$-*g*-OPhe, and $mPEG_{1000}$-*g*-OPhe were 0.3, 0.5, and 1.0 mg/mL, respectively.

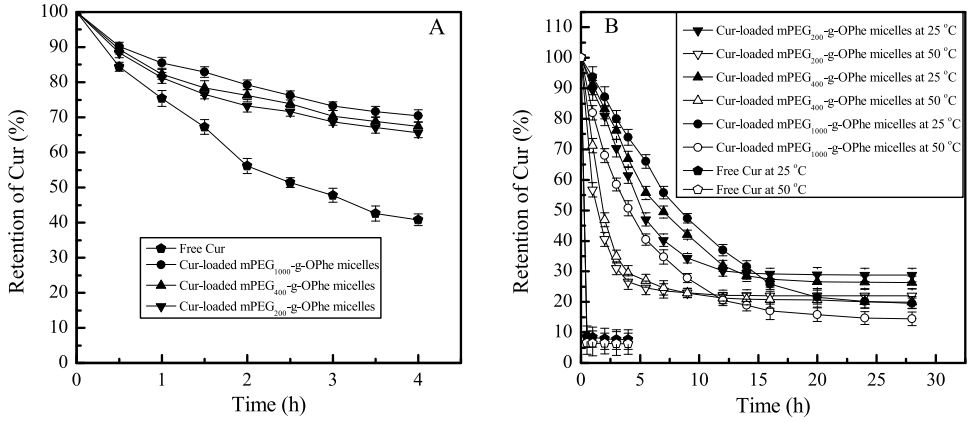

Figure 10. Light stability (A) of the Cur-loaded mPEG-*g*-OPhe NP micelles at 25 °C and pH 7.0 and the encapsulation stability (B) of the Cur-loaded mPEG-*g*-OPhe NP micelles at 25 °C and 50 °C, respectively, at pH 7.0. The concentrations of $mPEG_{200}$-*g*-OPhe, $mPEG_{400}$-*g*-OPhe, and $mPEG_{1000}$-*g*-OPhe were 0.3, 0.5, and 1.0 mg/mL, respectively.

micellar aggregation of mPEG-*g*-OPhe NPs in water increased when the chain length of the mPEG moiety increased. In the case of reverse micelles, the hydrophilic mPEG chains of mPEG-*g*-OPhe NPs shrank and fused to form the hydrophilic core in cyclohexane driven by the interfacial tension and free energy. The average diameter of the reverse micelles in CyH increased slightly, by about 14.3% (Table S3), when the MW of the mPEG moiety increased from 200 to 1000. The CRMC for the micellar aggregation of mPEG-*g*-OPhe NPs in CyH decreased when the chain length of the mPEG moiety increased.

Stability of the Payload Encapsulated in the Micelles Formed by mPEG-*g*-OPhe NPs. The solubilization of hydrophobic substances is an important issue in the industry of food, cosmetics, pharmaceuticals, and in many other fields.[53,54] The hydrophobic inner core of micelles can physically incorporate water-insoluble payloads by hydrophobic interactions. The hydrophilic shells of micelles afford the encapsulated payload solubility in water. Herein, the encapsulating capacity of the micelles formed by mPEG-*g*-OPhe NPs was investigated using curcumin (Cur) as the model payload. Curcumin (Cur), known chemically as 1,7-bis(4-hydroxy-3-methoxyphenyl)-1,6- heptadiene-3,5-dione, is poorly soluble in aqueous media.[55] It is used as a dietary supplement in Southeast Asia and has versatile biological and pharmacological activities such as anticancer, antioxidant, antimicrobial, antiparasitic, etc.[56] The aqueous solubility of curcumin can be improved by increasing the pH of the solution. However, this approach leads to the rapid degradation of Cur by alkaline hydrolysis.[57]

Transmission electron microscopy (TEM) images (Figure 9) show that the spherical Cur-loaded micelles formed by mPEG-*g*-OPhe NPs are polydisperse. When encapsulated, the aromatic moieties of Cur bind the hydrophobic core of the micelles formed by mPEG-*g*-OPhe NPs through aromatic staking interactions. The $R_{h,m}$ values were determined to be 420.3 ± 19.8, 496.2 ± 20.2, and 636.1 ±2.7 nm at 25 °C for the Cur-loaded micelles stabilized by $mPEG_{200}$-*g*-OPhe NPs, $mPEG_{400}$-*g*-OPhe NPs, and $mPEG_{1000}$-*g*-OPhe NPs, respectively (Table S4). The micellar hydrodynamic radius is larger than the average radius observed by TEM, because the micelles were dried and shrank in the drying treatment before TEM observation. The micelles formed by $mPEG_{200}$-*g*-OPhe NPs had the highest encapsulation efficiency based on the value of LE (Table S4). The Cur-loaded micelles formed by mPEG-*g*-OPhe NPs are stable for at least 30 days without any detectable significant changes in the appearances, LE values, and $R_{h,m}$ values (Figure 9 and Table S4).

The encapsulation in the micelles formed by mPEG-*g*-OPhe NPs significantly increased the resistance of Cur against photodegradation (Figure 10A). After 4 h of light exposure, the retention of Cur was increased by about 60.8% by the

https://dx.doi.org/10.1021/acsomega.0c05076
ACS Omega 2020, 5, 30336−30347

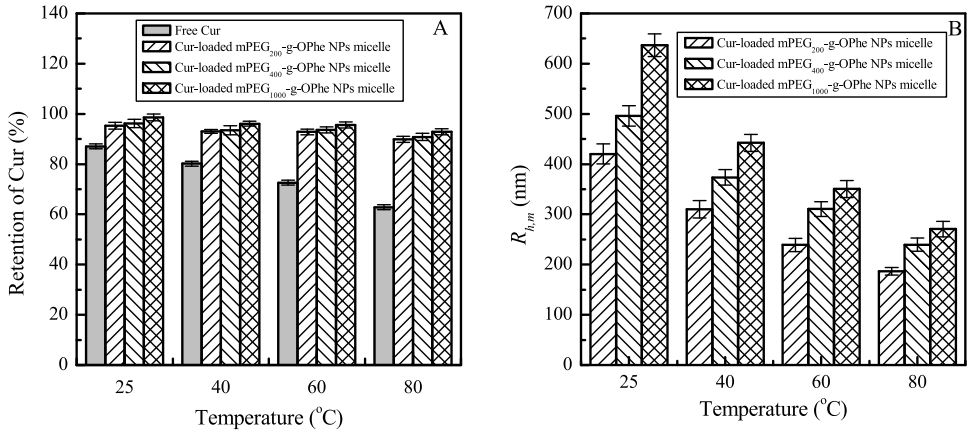

Figure 11. Thermal stability (A) and $R_{h,m}$ (B) of the Cur-loaded micelles formed by mPEG-*g*-OPhe NPs in the temperature range of 25 to 80 °C at pH 7.0 for 2 h. The concentrations of $mPEG_{200}$-*g*-OPhe, $mPEG_{400}$-*g*-OPhe, and $mPEG_{1000}$-*g*-OPhe were 0.3, 0.5, and 1.0 mg/mL, respectively.

encapsulation in $mPEG_{200}$-*g*-OPhe NP micelles, 65.4% in $mPEG_{400}$-*g*-OPhe NP micelles, and 72.5% in $mPEG_{1000}$-*g*-OPhe NP micelles, respectively. The thicker hydrophilic shell formed by the longer mPEG chain may account for the higher light stability of Cur-loaded micelles. The encapsulation on the release rate of Cur from the dialysis bag at 25 °C and 50 °C, respectively, were evaluated and the results are shown in Figure 10B. The percentage of released Cur from the dialysis bag in 0.5 h decreased from 90 ± 3.2% (free Cur powder) to 11.1 ± 1.2% (Cur-loaded $mPEG_{200}$-*g*-OPhe NP micelles), 9.2 ± 1.2% (Cur-loaded $mPEG_{400}$-*g*-OPhe NP micelles), and 5.4 ± 1.2% (Cur-loaded $mPEG_{1000}$-*g*-OPhe NP micelles) at 25 °C. The release of Cur reached the maximal value of 71.18 ± 1.73% in 12 h for Cur-loaded $mPEG_{200}$-*g*-OPhe NP micelles, 73.66 ± 2.11% in 16 h for Cur-loaded $mPEG_{400}$-*g*-OPhe NP micelles, and 80.48 ± 2.24% in 20 h for Cur-loaded $mPEG_{1000}$-*g*-OPhe NP micelles, respectively, at 25 °C. When the temperature rose to 50 °C, the release of Cur levelled off in about 5 h for Cur-loaded $mPEG_{200}$-*g*-OPhe NP micelles and Cur-loaded $mPEG_{400}$-*g*-OPhe NP micelles, and in about 12 h for Cur-loaded $mPEG_{1000}$-*g*-OPhe NP micelles (Figure 10B). At an elevated temperature, H bonds in the mPEG shell of the micelles become less stable, destabilizing the aggregation of the hydrophobic core and promoting the release of Cur. Besides, the motion of Cur molecules located in the micellar core was aggravated at higher temperatures, leading to the faster release from the micelles. This effect of varying chain lengths of the mPEG moiety of mPEG-*g*-OPhe NPs on the release of the payload from the micelles offers the possibility to manage the release, which is very valuable for technological applications.

It was also found the thermal stability of Cur was enhanced by encapsulation in the micelles formed by mPEG-*g*-OPhe NPs (Figure 11). The retention of Cur without encapsulation decreased from 87.16 ± 1.21% at 25 °C to 62.92 ± 1.13% at 80 °C after 2 h of incubation. When encapsulated, the retention of Cur can maintain at 90.18 ± 1.21% ($mPEG_{200}$-*g*-Ophe NP micelles), 92.87 ± 1.41% ($mPEG_{400}$-*g*-OPhe NP micelles) and 93.95 ± 1.21% (mPEG1000-*g*-OPhe NP micelles) at 80 °C, respectively. The $R_{h,m}$ of Cur-loaded micelles demonstrated a significant decrease when the temperature increased from 25 to 80 °C (Figure 11B). When the temperature was elevated, the hydrogen bonding between the mPEG chains and the surrounding water molecules weakened. The mPEG shell of the micelles collapsed repelling water molecules. The micelles shrank and became tight resulting in the decreased size.[58,59] The tightening of the micelles increased the shell density of micelles contributing to the enhanced protective effect stabilizing the Cur-loaded micelles at the elevated temperature. By adjusting the pH with 0.1 mol/L NaOH and 0.1 mol/L HCl, the effects of pH variation on the stability of Cur-loaded micelles were evaluated. The micellar encapsulation could significantly increase the hydrolysis stability of Cur in aqueous solution (Figure S24). After incubation at pH 10.0 for 20 h, the retention of Cur was increased by about 87.9, 93.4, and 99.5% when encapsulated with $mPEG_{200}$-*g*-OPhe NPs, $mPEG_{400}$-*g*-OPhe NPs, and $mPEG_{1000}$-*g*-OPhe NPs, respectively (Figure S24).

■ CONCLUSIONS

In this study, amphiphilic peptide nanoparticles, mPEG-*g*-OPhe NPs, were fabricated using papain. The $R_{h,m}$ value of OPhe NPs dispersed in an aqueous solution was about 200 nm after using SDS and urea to disrupt the hydrophobic interaction and hydrogen bonding between peptide chains. OPhe NPs are amphiphobic because of the Tyndall phenomena of their dispersion in water and organic solvents like cyclohexane, dioxane, chloroform, and methanol. Then, OPhe NPs were converted to mPEG-*g*-Ophe NPs by introducing mPEG at the N-terminal of OPhe NPs at the degree of substitution of 1 by ^{1}H NMR analysis. ATR-FTIR analysis revealed that the secondary structure of OPhe NPs and mPEG-*g*-OPhe NPs were mainly *β*-type. mPEG-*g*-OPhe NPs were able to self-assemble into micelles in water and cyclohexane. With the increase of the mPEG chain length, the CMC for mPEG-*g*-OPhe NPs in water increased, while the CRMR for mPEG-*g*-OPhe NPs in cyclohexane decreased. The light stability, thermal stability, encapsulation stability, and the hydrolysis stability of Cur were significantly improved by encapsulation in the micelles formed by mPEG-*g*-OPhe NPs. The influence of varying the chain length of mPEG on the stability of Cur encapsulated in the micelles formed by mPEG-*g*-OPhe NPs offers the possibility to manage the encapsulation for technological applications. Considering their biocompatibility,[60,61] mPEG-*g*-OPhe NPs and their micellar self-aggregations hold much promise for a range of potential applications in medicine, food science, cosmetics, and nanotechnology.

https://dx.doi.org/10.1021/acsomega.0c05076
ACS Omega 2020, 5, 30336−30347

MATERIALS AND METHODS

Materials. Papain (EC 3.4.22.2, ≥10 U/mg) was purchased from Shanghai Aladdin Bio-Chem Technology Co., LTD. L-Phenylalanine methyl ester hydrochloride (L-Phe-OMe·HCl, 98%), Brij L4 (average $M_n \sim 362$), curcumin (≥80%), Nile red (≥98.0%), Rhodamine B (98%), and iodine (≥99.99%) were purchased from Sigma-Aldrich. Methoxypolyethylene glycol succinimidyl carbonate ester ($mPEG_{200}$-SC, $mPEG_{400}$-SC, and $mPEG_{1000}$-SC), derived from mPEGs of different molecular weights (200, 400, and 1000 Da), were purchased from Nanocs Inc. Dimethyl sulfoxide (DMSO, >99.9%), dioxane (Diox, >99.5%), methanol (MeOH, 99.7%), tetrahydrofuran (THF, ≥99.9%), *N*,*N*-dimethylformamide (DMF, 99.8%), hexafluoroisopropanol (HFIP, 99.5%), acetonitrile (ACN, ≥99.9%), triethylamine (≥99.5%), cyclohexane (CyH, ≥99.5%), and deuterated dimethyl sulfoxide (DMSO-d_6, D, 99.9% + 0.05% TMS) were obtained from Shanghai Aladdin Bio-Chem Technology Co., LTD. All other chemicals were analytically pure and purchased from Sinopharm Chemical Reagent Co.

Synthesis of OPhe NPs. L-Phe-OMe·HCl (200 mg/mL) and 4 U/mL papain were added to 3.0 mL of phosphate buffer (pH = 8.0, 200 mmol/L) containing 15% (v/v) DMSO. The reaction was carried out at 40 °C for 3 h. At the end of the reaction, the reaction mixture was poured into 10 mL of icy distilled water. After centrifugation, the precipitate was collected and washed with icy distilled water five times. The precipitate was lyophilized to obtain oligo-phenylalanine nanoparticles (OPhe NPs). Control experiments performed without addition of the enzyme did not yield any precipitate. On the basis of the weight of the dried product, the yield of OPhe NPs was determined according to the amount of OPhe NPs produced per 100 grams of L-Phe-OMe·HCl.

The optimization of the oligomerization was performed in 3.0 mL of buffer solution containing 4 U/mL papain. The influences of various initial concentrations of L-Phe-OMe·HCl (from 50 mg/mL to 350 mg/mL), cosolvents (from 5 to 40%, v/v), temperatures (from 25 to 55 °C), pHs (from 5.5 to 10), and the reaction times (from 0.5 h to 6 h) were evaluated. Citrate buffers (pH 5.5−6.0, 200 mmol/L), phosphate buffers (pH 6.5−8.0, 200 mmol/L), and borate buffers (pH 8.5−10, 200 mmol/L) were used for reactions at different pH values. The data shown in the figures are the average values from triplicate experiments and include standard deviations.

Preparation of mPEG-*g*-OPhe NPs. In 30 mL of 30 mg/mL suspension in methanol of OPhe NPs, 110 mmol/L mPEG-SC, and 150 mmol/L trimethylamine were added under a N_2 atmosphere. The reaction was conducted with stirring for 48 h at 25 °C. At the end of the reaction, the reaction mixture was dialyzed against pure water for 48 h using a dialysis cellulose membrane bag (MW cutoff 1000 Da) to remove *N*-hydroxysuccinimide, triethylamine, and other small molecules with frequent changes of the water. The inner solution was concentrated under vacuum and freeze-dried. The dried product was washed with icy ethanol and acetone successively to remove the remaining mPEG-SC until no mPEG-SC was detected by mass spectrometry. One gram of OPhe NPs can be converted to 1.03 ± 0.05 g of $mPEG_{200}$-*g*-OPhe NPs, 1.15 ± 0.12 g of $mPEG_{400}$-*g*-OPhe NPs, and 1.65 ± 0.15 g of $mPEG_{1000}$-*g*-OPhe NPs.

Normal Micelles Stabilized by mPEG-*g*-OPhe NPs. Micellar self-aggregation of mPEG-*g*-OPhe NPs in water was investigated with Nile red as the fluorescent probe.[46,62] Nile red stock solution (20 μL (1 mmol/L) in methanol) was transferred into a glass vial (φ25 × 75 mm). The solvent was carefully removed by nitrogen flushing leaving brick red thin solid films. Then, 7 mL of the mPEG-*g*-OPhe NP suspension in distilled water was added into the vial. After 12 h of magnetic stirring at room temperature, fluorescence measurements were carried out on a Hitachi F4500 fluorescence spectrophotometer (Japan). Emission spectra were recorded from 550 to 750 nm using λ_{exc} = 550 nm. Excitation and emission slit widths were both maintained at 5.0 nm. Spectra were accumulated with a scan speed of 200 nm/min. The value of critical micellar concentration (CMC) was determined at the inflection point in the plots representing the maximum emission wavelength as a function of the concentration of mPEG-*g*-OPhe NPs.

Reverse Micelle Stabilized by mPEG-*g*-OPhe NPs. The reversed micelles of mPEG-*g*-OPhe NPs in cyclohexane were prepared according to the method reported in the literature.[48] Cyclohexane solution (9.4 mL) of mPEG-*g*-OPhe NPs and Brij L4 was transferred into a glass vial (φ25 × 75 mm). The molar ratio of mPEG-*g*-OPhe NPs to Brij L4 was 1:1. Then, 0.6 mL of I_2 solution (0.1 mg/mL in cyclohexane) was added into the vial. Iodine was sublimed before use. After 2 h of ultrasonic treatment on an SB-5200 DTN Sonicator (Ningbo Xinzhi Biotechnology Co., Ltd.) at 25 °C, the absorption intensity of the reverse micelles were recorded at around 370 nm using a Shimadzu-3100 double beam spectrophotometer (Japan). The value of critical reverse micelle concentration (CRMC) was determined at the inflection point in the plot of the absorption intensity as the function of the mPEG-*g*-OPhe NP concentration. For obtaining the fluorescence images of dye-impregnated reverse micelles formed by mPEG-*g*-OPhe NPs, Rhodamine B was used as the laser dye. In a glass vial (φ18 × 40 mm), 5 mL of the micelles formed by mPEG-*g*-OPhe NPs in cyclohexane was mixed with 12.5 μL of Rhodamine B solution (2.67 mg/mL in BrijL4). The mixture was subjected to ultrasonic treatment (200 W) for 2 h at 25 °C. The concentrations of $mPEG_{200}$-*g*-OPhe NPs, $mPEG_{400}$-*g*-OPhe NPs, and $mPEG_{1000}$-*g*-OPhe NPs in cyclohexane were 0.45, 0.25, and 0.15 mg/mL, respectively. After that, Rhodamine B-stained reverse micelles formed by mPEG-*g*-OPhe NPs were imaged by CLSM.

Stability of the Payload Encapsulated in the Normal Micelles of mPEG-*g*-OPhe NPs. The effect of encapsulation in the micelles formed by mPEG-*g*-OPhe NPs on the stability of the payload was investigated using curcumin as the model. Curcumin (Cur) in ethanol (200 μL of 15 mg/mL) was added into a glass vial (φ25 × 75 mm). The solvent was removed by nitrogen flushing. Then, 5 mL of the mPEG-*g*-OPhe NP micelle solution was added into the vial. The concentrations of $mPEG_{200}$-*g*-OPhe, $mPEG_{400}$-*g*-OPhe, and $mPEG_{1000}$-*g*-OPhe were 0.45, 0.65, and 1.5 mg/mL, respectively. After 2 h of ultrasonic treatment on a SB-5200 DTN Sonicator (Ningbo Xinzhi Biotechnology Co., Ltd.) at 200 W and 25 °C, the vials were rotated end-over-end on a HS-3 Rotary Mixer (Ningbo Xinzhi Biotechnology Co., Ltd.) at 20 rpm overnight, at 25 °C. After that, the undissolved Cur was removed by centrifugation (4000 rpm, 10 min) and filtration through a 0.8 μm filter membrane. An aliquot of Cur-loaded micelle solution (10 μL) was diluted to 1 mL with ethanol to determine the absorption intensity at 428 nm. The quantity of Cur was determined according to the calibration curve of Cur in ethanol made at

https://dx.doi.org/10.1021/acsomega.0c05076
ACS Omega 2020, 5, 30336−30347

428 nm in the concentration range of 1.0−6.0 μg/mL. The payload loading efficiency (LE) was calculated by the following equation

$$\text{LE}\ (\%) = \frac{m_1}{m_1 + m_2} \times 100$$

where m_1 is the weight of Cur in the micelle solution and m_2 is the weight of mPEG-*g*-OPhe NPs stabilizing the micelle.

The photochemical stability of free Cur (1 mg/mL in ethanol) and the Cur-loaded micelle solution was determined using an illumination method in a light cabinet (ZSW-Q100, Zhenxiang Electrical Technology (Shanghai) Co., Ltd) at 30 °C.[63] The light intensity was set at 5000 lux and 5 W/m^2. At regular intervals, the quantity of Cur in the micellar samples was determined according to the aforementioned method. Each sample was analyzed in triplicate.

The thermal stability of free Cur (1 mg/mL in propylene glycol) and the Cur-loaded micelle solution was determined in a thermostatic water bath at temperatures of 25, 40, 60, and 80 °C for 2 h. At regular intervals, the quantity of Cur in the micellar samples was determined according to the aforementioned method. Each sample was analyzed in triplicate.

The encapsulation stability of Cur-loaded mPEG-*g*-OPhe NP micelles was examined by a dialysis method. 5 mL of the Cur-loaded micelle solution was transferred to a dialysis bag (MWCO = 500 Da) and dialyzed against 2% (w/v) Triton X-100 in PBS buffer for 28 h in the temperature range of 20 to 50 °C. The PBS buffer (pH = 7.4) was composed of 137 mmol/L NaCl, 10 mmol/L Na_2HPO_4, 2.68 mmol/L KCl, and 1.84 mmol/L KH_2PO_4.[64] At an interval of 30 min, 5 mL of the sample was withdrawn from the dialysate and replaced with the same volume of fresh 2% (w/v) Triton X-100 PBS buffer. The Cur concentration in the samples was measured. Values are means of three parallel experiments. Retention of Cur was calculated by dividing the Cur concentration of samples by the initial concentration of Cur in the Cur-loaded micelles stabilized by mPEG-*g*-OPhe NPs.

Tyndall Effect. The suspension of OPhe NPs and mPEG-*g*-OPhe NPs was treated with ultrasonic treatment on a SB-5200 DTN Sonicator (Ningbo Xinzhi Biotechnology Co., Ltd.) at the power output of 200 W for 2 h at room temperature. The Tyndall effect was utilized to confirm the existence of nanoparticles in the solutions using a 1 mW 635 nm red laser pointer as the light source. A visible light beam path can be observed in the nanoparticle solution due to Tyndall scattering.

Scanning Electron Microscopy of OPhe NPs. The morphology of OPhe NPs was examined by scanning electron microscopy (SEM). After lyophilization, OPhe NPs were coated with a 2 nm layer of gold and imaged using an S-4800 scanning electron microscope (Hitachi Ltd., Tokyo, Japan).

Pattern of Intraparticle Interactive Forces. The pattern of interactive forces between peptide chains involved in the formation and maintenance of OPhe NPs was determined by monitoring the changes in the particle size of the OPhe NP dispersions in different solvents: distilled water, 4% (w/v) SDS, and 8 M urea, alone or in combination.

Attenuated Total Reflectance Fourier Transform Infrared Spectroscopy (ATR-FTIR). ATR was performed on a Nicolet 6700 spectrometer (Thermo) equipped with a Smart Multi-Bounce Horizontal Attenuated Total Reflectance (HATR) device having zinc selenide (ZnSe) crystals. Spectra were recorded in the 4000−400 cm^{-1} range at a resolution of 2 cm^{-1}, averaging 32 scans per sample. The background spectrum was subtracted from the sample spectrum using the Nicolet software. Second-derivative spectra were obtained using the OMNIC software program (version 7.0, Thermo Fisher Scientific, Waltham) following the Savitsky−Golay method.[65] Curve fitting of the amide I band from 1700 to 1600 cm^{-1} was performed by OMNIC software as a linear combination of Gaussian components. In the fitting, the number of components and initial values of their peak positions were obtained from the second derivative spectra.

^{1}H NMR. ^{1}H NMR spectra of mPEG-*g*-OPhe NPs were obtained using a Bruker AVANCE HD-400 MHz spectrometer. The samples were dissolved in deuterated dimethyl sulfoxide (DMSO-d_6) containing 1% (w/v) trifluoroacetic acid (TFA) at 10 mg/mL. Tetramethylsilane (TMS) was used as the internal reference at 0.00 ppm. A total of 128 scans were recorded. Data were collected and analyzed by MestReNova software. Proton chemical shifts were referenced to TMS at 0.00 ppm.

Mass Spectrometry. OPhe NPs and mPEG-*g*-OPhe NPs were dissolved in DMSO at 1 mg/mL. The solutions were introduced into the electrospray source of a Micromass Platform LCZ/2690XE/996 spectrometer operated in positive ion mode (Waters, Milford) with a cone voltage of 20 V. The ion source temperature was 100 °C. The desolvation gas was nitrogen at 350 L/h. Mass spectra were recorded over the mass range of m/z 200−4500 with a scan rate of 0.5 Hz. Data were collected and analyzed by Masslynx software.

Dynamic Light Scattering (DLS) Measurements. Dynamic light-scattering (DLS) measurements were conducted with a laser light-scattering spectrometer ALV/DLS/SLS-5022F (ALV Co., Germany) at an angle of 90°. The light source was a cylindrical He−Ne laser (model 1145p-3083, output power = 22 mW at λ = 632.8 nm). The laser light-scattering cell was held in a thermostat index-matching vat filled with purified dust-free toluene. At each temperature the sample was kept for 10 min to reach equilibrium. The time correlation functions were analyzed with a Laplace inversion program (CONTIN). Each experiment was repeated two or more times.

Confocal Laser Scanning Microscopy. The microstructures of Nile red-loaded micelles in water and Rhodamine B-loaded micelles in cyclohexane stabilized by mPEG-*g*-OPhe NPs were observed with a Carl Zeiss TCS SP8 confocal laser scanning microscope (Leica Microsystems Inc., Heidelberg, Germany) using a 63× oil immersion objective with a numerical aperture (NA) of 1.4. Emission spectra of Nile red and Rhodamine B were recorded from 550 to 750 nm at the excitation wavelengths of (λ_{exc}) 543 nm and 552 nm, respectively.

Transmission Electron Microscopy. The morphological characteristics of OPhe NPs and the Cur-loaded micelles formed by mPEG-*g*-OPhe NPs were observed using a transmission electron microscope (TEM, JEM-2100plus, JEOL, Tokyo, Japan) at the accelerating voltage of 200 kV. The micellar solution was deposited onto a carbon-coated copper grid (300 mesh) and stained with phosphotungstic acid solution (2%, w/v) for about 15 s to prepare the samples for TEM. Then, the sample was dried at room temperature for 60 s and examined under a TEM.

https://dx.doi.org/10.1021/acsomega.0c05076
ACS Omega 2020, 5, 30336−30347

■ ASSOCIATED CONTENT

Supporting Information

The Supporting Information is available free of charge at https://pubs.acs.org/doi/10.1021/acsomega.0c05076.

Solid-state ATR spectrum; ^{1}H NMR spectra; ESI-MS; absorbance spectra of iodine in the mPEG-*g*-OPhe NPs/CyH solution; $R_{h,m}$; and retention of Cur at different pHs (PDF)

■ AUTHOR INFORMATION

Corresponding Author

Feng Wang − *Key Laboratory of Synthetic and Biological Colloids, Ministry of Education and School of Chemical and Material Engineering, Jiangnan University, Wuxi 214122, China;* orcid.org/0000-0002-0482-3720; Email: fwang@jiangnan.edu.cn

Authors

Youhua Li − *School of Chemical and Material Engineering, Jiangnan University, Wuxi 214122, China*

Lu Yu − *School of Chemical and Material Engineering, Jiangnan University, Wuxi 214122, China*

Jinwen Zhu − *School of Chemical and Material Engineering, Jiangnan University, Wuxi 214122, China*

Fuming Zhang − *Department of Chemistry and Chemical Biology, Departments of Chemical and Biological Engineering, Biology and Biomedical Engineering, Center for Biotechnology and Interdisciplinary Studies, Rensselaer Polytechnic Institute, Troy, New York 12180, United States;* orcid.org/0000-0003-2803-3704

Robert J. Linhardt − *Department of Chemistry and Chemical Biology, Departments of Chemical and Biological Engineering, Biology and Biomedical Engineering, Center for Biotechnology and Interdisciplinary Studies, Rensselaer Polytechnic Institute, Troy, New York 12180, United States;* orcid.org/0000-0003-2219-5833

Complete contact information is available at: https://pubs.acs.org/10.1021/acsomega.0c05076

Notes

The authors declare no competing financial interest.

■ REFERENCES

(1) Diaferia, C.; Mercurio, F. A.; Giannini, C.; Sibillano, T.; Morelli, G.; Leone, M.; Accardo, A. Self-assembly of PEGylated tetraphenylalanine derivatives: structural insights from solution and solid state studies. *Sci. Rep.* **2016**, *6*, No. 26638.

(2) Yu, J.; Horsley, J. R.; Abell, A. D. Peptides as bio-inspired electronic materials: an Electrochemical and first-principles perspective. *Acc. Chem. Res.* **2018**, *51*, 2237−2246.

(3) Merrifield, R. Solid-phase peptide synthesis. *Adv. Enzymol. Relat. Areas Mol. Biol.* **1969**, *32*, 221−296.

(4) Merrifield, B. Solid Phase Synthesis. *Science* **1986**, 232, 341−347.

(5) Hancock, R. E. W. Cationic peptides: effectors in innate immunity and novel antimicrobials. *Lancet Infect. Dis.* **2001**, *1*, 156−164.

(6) Tsuchiya, K.; Numata, K. Chemoenzymatic synthesis of polypeptides for use as functional and structural materials. *Macromol. Biosci.* **2017**, *17*, No. 1700177.

(7) Qin, X.; Xie, W.; Su, Q.; Du, W.; Gross, R. A. Protease-catalyzed oligomerization of l-lysine ethyl ester in aqueous solution. *ACS Catal.* **2011**, *1*, 1022−1034.

(8) Xu, S.; Zhao, Z.; Zhao, J. Recent advances in enzyme-mediated peptide ligation. *Chin. Chem. Lett.* **2018**, *29*, 1009−1016.

(9) Hamley, I. W. PEG-peptide conjugates. *Biomacromolecules* **2014**, *15*, 1543−1559.

(10) Perinelli, D. R.; Campana, M.; Singh, I.; Vllasaliu, D.; Doutch, J.; Palmieri, G. F.; Casettari, L. PEGylation affects the self-assembling behaviour of amphiphilic octapeptides. *Int. J. Pharm.* **2019**, *571*, No. 118752.

(11) Kumar, S.; Hause, G.; Binder, W. H. Bifunctional peptide-polymer conjugate-based fibers via a one-pot tandem disulfide reduction coupled to a thio-bromo "click" reaction. *ACS Omega* **2020**, *5*, 19020−19028.

(12) Tzokova, N.; Fernyhough, C. M.; Topham, P. D.; Sandon, N.; Adams, D. J.; Butler, M. F.; Armes, S. P.; Ryan, A. J. Soft hydrogels from nanotubes of poly(ethylene oxide)-tetraphenylalanine conjugates prepared by click chemistry. *Langmuir* **2009**, *25*, 2479−2485.

(13) Dong, H.; Dube, N.; Shu, J. Y.; Seo, J. W.; Mahakian, L. M.; Ferrara, K. W.; Xu, T. Long-circulating 15 nm micelles based on amphiphilic 3-helix peptide-PEG conjugates. *ACS Nano* **2012**, *6*, 5320−5329.

(14) Tzokova, N.; Fernyhough, C. M.; Butler, M. F.; Armes, S. P.; Ryan, A. J.; Topham, P. D.; Adams, D. J. The effect of PEO length on the self-assembly of poly(ethylene oxide)-tetrapeptide conjugates prepared by "click" chemistry. *Langmuir* **2009**, *25*, 11082−11089.

(15) Zaman, M.; Ahmad, E.; Qadeer, A.; Rabbani, G.; Khan, R. H. Nanoparticles in relation to peptide and protein aggregation. *Int. J. Nanomed.* **2014**, *9*, 899−912.

(16) Zhang, Y.; Zhou, F.; Zhao, M.; Lin, L.; Ning, Z.; Sun, B. Soy peptide nanoparticles by ultrasound-induced self-assembly of large peptide aggregates and their role on emulsion stability. *Food Hydrocolloids* **2018**, *74*, 62−71.

(17) Frederix, P. W. J. M.; Scott, G. G.; Abul-Haija, Y. M.; Kalafatovic, D.; Pappas, C. G.; Javid, N.; Hunt, N. T.; Ulijn, R. V.; Tuttle, T. Exploring the sequence space for (tri-)peptide self-assembly to design and discover new hydrogels. *Nat. Chem.* **2015**, *7*, 30−37.

(18) Rymer, S.-J.; Tendler, S. J.; Bosquillon, C.; Washington, C.; Roberts, C. J. Self-assembling peptides and their potential applications in biomedicine. *Ther. Delivery* **2011**, *2*, 1043−1056.

(19) Wang, W.; Yang, Z.; Patanavanich, S.; Xu, B.; Chau, Y. Controlling self-assembly within nanospace for peptide nanoparticle fabrication. *Soft Matter* **2008**, *4*, 1617−1620.

(20) Zhang, J.; Zhao, Y.; Han, S.; Chen, C.; Xu, H. Self-assembly of surfactant-like peptides and their applications. *Sci. China: Chem.* **2014**, *57*, 1634−1645.

(21) Liu, L.; Xu, K.; Wang, H.; Jeremy Tan, P. K.; Fan, W.; Venkatraman, S. S.; Li, L.; Yang, Y.-Y. Self-assembled cationic peptide nanoparticles as an efficient antimicrobial agent. *Nat. Nanotechnol.* **2009**, *4*, 457−463.

(22) Yaman, Y. T.; Akbal, Ö.; Bolat, G.; Bozdogan, B.; Denkbas, E. B.; Abaci, S. Peptide nanoparticles (PNPs) modified disposable platform for sensitive electrochemical cytosensing of DLD-1 cancer cells. *Biosens. Bioelectron.* **2018**, *104*, 50−57.

(23) Zhang, H.; Fei, J.; Yan, X.; Wang, A.; Li, J. Enzyme-responsive release of doxorubicin from monodisperse dipeptide-based nanocarriers for highly efficient cancer treatment in vitro. *Adv. Funct. Mater.* **2015**, *25*, 1193−1204.

(24) Dittrich, C.; Meier, W. Solid peptide nanoparticles-structural characterization and quantification of cargo encapsulation. *Macromol. Biosci.* **2010**, *10*, 1406−1415.

(25) Aiertza, M. K.; Odriozola, I.; Cabañero, G.; Grande, H.-J.; Loinaz, I. Single-chain polymer nanoparticles. *Cell. Mol. Life Sci.* **2012**, *69*, 337−346.

(26) Marques, C. M. Bunchy Micelles. *Langmuir* **1997**, *13*, 1430−1433.

(27) Centore, R.; Totsingan, F.; Amason, A.-C.; Lyons, S.; Zha, R. H.; Gross, R. A. Self-assembly-assisted kinetically controlled papain-catalyzed formation of mPEG-b-Phe(Leu)x. *Biomacromolecules* **2020**, *21*, 493−507.

(28) Ageitos, J. M.; Baker, P. J.; Sugahara, M.; Numata, K. Proteinase K-catalyzed synthesis of linear and star oligo(L-phenylalanine) conjugates. *Biomacromolecules* **2013**, *14*, 3635−3642.

(29) Uyama, H.; Fukuoka, T.; Komatsu, I.; Watanabe, T.; Kobayashi, S. Protease-catalyzed regioselective polymerization and copolymerization of glutamic acid diethyl ester. *Biomacromolecules* **2002**, *3*, 318−323.
(30) Ekinci, D.; Şentürk, M. Interactions of Fungicides and Pesticides with Specific Enzymes. In *Fungicides*; In-Tech, 2010; pp 383−404.
(31) Yang, F.; Totsingan, F.; Dolan, E.; Khare, S. D.; Gross, R. A. Protease-catalyzed l-aspartate oligomerization: substrate selectivity and computational modeling. *ACS Omega* **2020**, *5*, 4403−4414.
(32) Viswanathan, K.; Omorebokhae, R.; Li, G.; Gross, R. A. Protease-catalyzed oligomerization of hydrophobic amino acid ethyl esters in homogeneous reaction media using L-phenylalanine as a model system. *Biomacromolecules* **2010**, *11*, 2152−2160.
(33) Li, G.; Vaidya, A.; Viswanathan, K.; Cui, J.; Xie, W.; Gao, W.; Gross, R. A. Rapid regioselective oligomerization of l-glutamic acid diethyl ester catalyzed by papain. *Macromolecules* **2006**, *39*, 7915−7921.
(34) Wang, F.; Zhu, J.; Yan, T.; Pei, X.; Zhang, F.; Linhardt, R. J. Amphiphilic bromelain-synthesized oligo-phenylalanine grafted with methoxypolyethylene glycol possessing stabilizing thermo-responsive emulsion properties. *J. Colloid Interface Sci.* **2019**, *538*, 1−14.
(35) Klibanov, A. M. Improving enzymes by using them in organic solvents. *Nature* **2001**, *409*, 241−246.
(36) Stevenson, D. E.; Storer, A. C. Papain in organic solvents: Determination of conditions suitable for biocatalysis and the effect on substrate specificity and inhibition. *Biotechnol. Bioeng.* **1991**, *37*, 519−527.
(37) Rootman, D. B.; Lin, J. L.; Goldberg, R. Does the Tyndall effect describe the blue hue periodically observed in subdermal hyaluronic acid gel placement? *Ophthalmic Plast. Reconstr. Surg.* **2014**, *30*, 524−527.
(38) Yoshida, H.; Yanagisawa, K. Creation of superhydrophobic poly(L-phenylalanine) nonwovens by electrospinning. *Polymers* **2018**, *10*, 1212.
(39) Chen, N.; Lin, L.; Sun, W.; Zhao, M. Stable and pH-sensitive protein nanogels made by self-assembly of heat denatured soy protein. *J. Agric. Food Chem.* **2014**, *62*, 9553−9561.
(40) Liu, K. S.; Hsieh, F.-H. Protein-protein interactions in high moisture-extruded meat analogs and heat-induced soy protein gels. *J. Am. Oil Chem. Soc.* **2007**, *84*, 741−748.
(41) Ellepola, S. W.; Choi, S. M.; Ma, C. Y. Conformational study of globulin from rice (*Oryza sativa*) seeds by Fourier-transform infrared spectroscopy. *Int. J. Biol. Macromol.* **2005**, *37*, 12−20.
(42) Paramonov, S. E.; Jun, H.-W.; Hartgerink, J. D. Self-assembly of peptide-amphiphile nanofibers: The roles of hydrogen bonding and amphiphilic packing. *J. Am. Chem. Soc.* **2006**, *128*, 7291−7298.
(43) Huang, L.; Nishinari, K. Interaction between poly(ethylene glycol) and water as studied by differential scanning calorimetry. *J. Polym. Sci., Part B: Polym. Phys.* **2001**, *39*, 496−506.
(44) Tang, C.-H.; Ma, C.-Y. Effect of high pressure treatment on aggregation and structural properties of soy protein isolate. *LWT - Food Sci. Technol.* **2009**, *42*, 606−611.
(45) Liang, Y.; Sun, Y.; Fu, X.; Lin, Y.; Meng, Z.; Meng, Y.; Niu, J.; Lai, Y.; Sun, Y. The effect of π-conjugation on the self-assembly of micelles and controlled cargo release. *Artif. Cells, Nanomed., Biotechnol.* **2020**, *48*, 525−532.
(46) Kurniasih, I. N.; Liang, H.; Mohr, P. C.; Khot, G.; Rabe, J. P.; Mohr, A. Nile red dye in aqueous surfactant and micellar solution. *Langmuir* **2015**, *31*, 2639−2648.
(47) Biasutti, M. A.; Sereno, L.; Silber, J. J. Interaction of iodine with aerosol-OT in reversed micelles in n-hexane. *J. Colloid Interface Sci.* **1994**, *164*, 410−415.
(48) Rakshit, R. K.; Veena, V. Study of reverse micellization of span 60 in toluene. *Bull. Chem. Soc. Jpn.* **1994**, *67*, 854−855.
(49) Sinkeldam, R. W.; Greco, N. J.; Tor, Y. Fluorescent analogs of biomolecular building blocks: Design, properties, and applications. *Chem. Rev.* **2010**, *110*, 2579−2619.
(50) Li, N.; Huang, G.; Xiao, H.; Feng, Q.; Fu, S. Investigations on structure-dependent microwave absorption performance of nano-Fe_3O_4 coated carbon-based absorbers. *Carbon* **2019**, *144*, 216−227.
(51) Cui, F.; Li, Y.; Zhou, S.; Jia, M.; Yang, X.; Yu, F.; Ye, S.; Hou, Z.; Xie, L. A comparative in vitro evaluation of self-assembled PTX-PLA and PTX-MPEG-PLA nanoparticles. *Nanoscale Res. Lett.* **2013**, *8*, 301.
(52) Pashkovskaya, A. A.; Lukashev, E. P.; Antonov, P. E.; Finogenova, O. A.; Ermakov, Y. A.; Melik-Nubarov, N. S.; Antonenko, Y. N. Grafting of polylysine with polyethylenoxide prevents demixing of O-pyromellitylgramicidin in lipid membranes. *Biochim. Biophys. Acta, Biomembr.* **2006**, *1758*, 1685−1695.
(53) Rezaei, A.; Fathi, M.; Jafari, S. M. Nanoencapsulation of hydrophobic and low-soluble food bioactive compounds within different nanocarriers. *Food Hydrocolloids* **2019**, *88*, 146−162.
(54) Ammala, A. Biodegradable polymers as encapsulation materials for cosmetics and personal care markets. *Int. J. Cosmet. Sci.* **2013**, *35*, 113−124.
(55) Anand, P.; Kunnumakkara, A. B.; Newman, R. A.; Aggarwal, B. B. Bioavailability of curcumin: Problems and promises. *Mol. Pharmaceutics* **2007**, *4*, 807−818.
(56) Parshad, B.; Yadav, P.; Kerkhoff, Y.; Mittal, A.; Achazi, K.; Haag, R.; Sharma, S. K. Dendrimer-based micelles as cyto-compatible nanocarriers. *New J. Chem.* **2019**, *43*, 11984−11993.
(57) Leung, M. H. M.; Colangelo, H.; Kee, T. W. Encapsulation of curcumin in cationic micelles suppresses alkaline hydrolysis. *Langmuir* **2008**, *24*, 5672−5675.
(58) Chen, J.; Liu, M.; Chen, C.; Gong, H.; Gao, C. Synthesis and characterization of silica nanoparticles with well-defined thermoresponsive PNIPAM via a combination of RAFT and click Chemistry. *ACS Appl. Mater. Interfaces* **2011**, *3*, 3215−3223.
(59) Nakayama, M.; Okano, T.; Miyazaki, T.; Kohori, F.; Sakai, K.; Yokoyama, M. Molecular design of biodegradable polymeric micelles for temperature-responsive drug release. *J. Controlled Release* **2006**, *115*, 46−56.
(60) Yu, L.; Chang, G. T.; Zhang, H.; Ding, J. D. Injectable block copolymer hydrogels for sustained release of a PEGylated drug. *Int. J. Pharm.* **2008**, *348*, 95−106.
(61) Gyenes, T.; Torma, V.; Gyarmati, B.; Zrínyi, M. Synthesis and swelling properties of novel pH-sensitive poly(aspartic acid) gels. *Acta Biomater.* **2008**, *4*, 733−744.
(62) Hong, H.; Mai, Y.; Zhou, Y.; Yan, D.; Cui, J. Self-assembly of large multimolecular micelles from hyperbranched star copolymers. *Macromol. Rapid Commun.* **2007**, *28*, 591−596.
(63) Wang, W.; Liu, F.; Gao, Y. Quercetagetin loaded in soy protein isolate−κ-carrageenan complex: Fabrication mechanism and protective effect. *Food Res. Int.* **2016**, *83*, 31−40.
(64) Naksuriya, O.; Shi, Y.; van Nostrum, C. F.; Anuchapreeda, S.; Hennink, W. E.; Okonogi, S. HPMA-based polymeric micelles for curcumin solubilization and inhibition of cancer cell growth. *Eur. J. Pharm. Biopharm.* **2015**, *94*, 501−512.
(65) Shao, Q.; Qian, Y.; Wu, P.; Zhang, H.; Cai, C. Graphene oxide-induced conformation changes of glucose oxidase studied by infrared spectroscopy. *Colloids Surf., B* **2013**, *109*, 115−120.

https://dx.doi.org/10.1021/acsomega.0c05076
ACS Omega 2020, 5, 30336−30347